Linear stability of needle crystals in the boundary-layer model of dendritic solidification

Fong Liu and Nigel Goldenfeld
Department of Physics and Materials Research Laboratory, University of Illinois at Urbana-Champaign, Urbana, Illinois 61801
(Received 19 November 1987)

We perform the linear-stability analysis in the boundary-layer model of dendritic solidification using both the direct matrix-diagonalization method and the differential-equation integration method. The fastest needle-crystal steady state is found to be linearly stable for nonzero anisotropy; successively slower needle crystals have successively more unstable modes. This result agrees with those previously obtained on other models.

I. INTRODUCTION

Complex structures are often observed in nonequilibrium systems, such as the dendritic crystals seen when solid grows from the undercooled melt,[1] or Saffman-Taylor fingers,[2,3] formed when one viscous fluid is displaced by another of lower density. Considerable progress has recently been made in the understanding of such systems.[4,5]

In dendritic solidification, a branched structure grows from the undercooled melt, with an approximately parabolic tip and sidebranches decorating the sides. The rate of growth of the dendrite is controlled by the rate of diffusion of latent heat of melting away from the solidification front. The dynamics is described by the diffusion equation together with appropriate boundary conditions[1]

$$\partial u/\partial t = D\nabla^2 u \ , \tag{1.1a}$$

$$v_n = -D\nabla u \cdot \hat{\mathbf{n}} \ , \tag{1.1b}$$

$$u_s = \Delta - d_0(\theta)k - \beta(\theta)v_n \ , \tag{1.1c}$$

where u is the dimensionless temperature field, D the diffusion constant, Δ the dimensionless undercooling, θ the angle between the normal to the curve and some fixed direction, and $d_0(\theta)$ the capillary length which may or may not be isotropic; v_n, k, and u_s are the normal velocity, curvature, and the temperature of the interface; the last term in Eq. (1.1c) accounts for the fact that the interface is not static.

This moving-boundary problem turns out to be quite difficult to solve and for this reason a variety of simpler models have been proposed,[6,7] one of which , the two-dimensional boundary-layer model (BLM),[8,9] is the subject of this article.

We shall be concerned with steady-state solutions of the BLM, and their stability. In the BLM and other models it is crucial to include the effect of crystalline anisotropy in the boundary condition Eq. (1.1c) in order that a steady-state, uniformly translating solution exists.[6,9] Such a steady-state solution is known as a needle crystal; loosely speaking, it corresponds to a dendrite without sidebranches. In the absence of surface tension and anisotropy, Eq. (1.1) possesses a continuous family of needle-crystal steady states known as the Ivantsov solution.[10]

These solutions are completely unstable because $d_0(\theta)=0$; furthermore, the existence of a continuous family of solutions rather than a single solution raises the problem of how the Ivantsov solution can be a zeroth-order approximation to experiment[11,12] or time-dependent computer simulation,[8] where only a single steady-state dendritic tip is observed for a wide class of initial conditions. This problem was resolved through the realization that surface tension is a singular perturbation.[9]

Once the surface tension and anisotropy are included, a discrete set of needle-crystal steady states with velocities $v_0, v_1, v_2, \ldots$ is selected from the continuum through a nontrivial solvability condition. The velocities v_i ($i=0,1,2,\ldots$) decrease with increasing index number i. However, only the fastest-moving needle crystal in this set corresponds to the tip of the dendrites reproducibly observed in the time-dependent computer simulations.[9]

The reason for this selection is believed to be due to the conjectured stability of these solutions, namely, that only the fastest solution is linearly stable while other solutions are unstable with a tip-splitting instability. The propose of this paper is to demonstrate that the conjectured stability spectrum does indeed occur within the BLM. This result is of particular interest because our linear-stability calculations are fully time dependent, and do not rely on a quasistatic approximation.

Our results supplement existing calculations on other models, which are valid either in a WKB approximation or in a quasistatic limit. Bensimon, Pelcé, and Shraiman[13] studied the discrete mode instability analytically using the WKB (Ref. 14) approximation for short-wavelength perturbations. They found that only the fastest solution of the discrete set is linearly stable and the ith solution has i unstable modes. Their results are valid for small Peclet numbers for dendritic growth. Kessler and Levine[15] studied the quasistatic limit of Eq. (1.1) and reached the same conclusion. However, the quasistatic approximation is true also only in the small-Peclet-number limit which implies small undercooling Δ. Their results do not extend to the case of greatest interest, namely, the case of vanishingly small anisotropy strength.

Here we present the linear-stability analysis for the BLM. We performed the calculations in two ways: the first using direct discretization of the stability operator, the second using a shooting technique originally developed by Mack[16] to study the Orr-Sommerfeld equation. The former technique is prohibitively expensive if one requires good reliability, and cannot be used for very small anisotropy. Our shooting technique is rapid and accurate. The two methods are in agreement over the range of anisotropy where they can be both performed; thus we believe that both techniques are either correct or incorrect. For very small anisotropy we use the shooting technique.

We found that the fastest needle crystal is indeed linearly stable for all nonzero anisotropy (and we give our bounds for this result later). The slower needle crystals are linearly unstable for all nonzero anisotropy, with the number of unstable modes equal to the index number of the needle crystal under consideration. Our results are entirely consistent with the previously mentioned calculations of other authors on other models.[13,15]

The results are, however, in disagreement with the conclusions reached by studying the time-dependent simulations[17,18] and assuming that the evolution of the system remained within the domain of the linearized dynamics. We believe that these calculations probe the nonlinear dynamics and so they cannot be directly compared with our results.

The BLM is believed to be a faithful representation of the dynamics of solidification for $\Delta \lesssim 1$. Our calculation is the first to treat the interface and diffusion field dynamics on equal footing, as one is obliged to do in the boundary-layer limit. Thus we expect that our results will apply to Eq. (1.1) in this regime. Our results complement those of Kessler and Levine,[15] which might reasonably by expected to apply to Eq. (1.1) in the limit $\Delta \to 0$. The conclusion is that sidebranching is either a nonlinear or noise-induced effect. Furthermore, as we and others have emphasized, velocity selection is not related to a stability principle.

The rest of the paper is organized as follows. In Sec. II we give the linear-stability-equation formalism of the BLM. In Sec. III we present the stability analysis for the Ivantsov solution of the BLM. This calculation is due to Goldenfeld and Langer.[19] In Secs. IV and V we present the results of the matrix method and integration (shooting) method respectively. Finally, Sec. VI is devoted to discussions.

II. BLM STABILITY ANALYSIS

The solidification front can be specified by its curvature $k(s,t)$ as a function of arclength s along the interface where $k(s,t)=\partial\theta/\partial s$. The following kinematical differential equations are exact in describing the front motion:

$$\left.\frac{\partial k}{\partial t}\right|_n = -\left[k^2+\frac{\partial^2}{\partial s^2}\right]v_n \ , \tag{2.1a}$$

$$\left.\frac{ds}{dt}\right|_n = \int_0^s k v_n ds' \ , \tag{2.1b}$$

where the subscript n indicates that the derivatives are made along the normal.

The excess latent heat released from solidification accumulates in a layer at the interface. If the thickness l of this layer is small compared with the local radius of curvature then we may simply consider the dynamics of l itself instead of the thermal field $u(x,t)$. This is the crux of the BLM approximation, which is good at large undercooling $\Delta \to 1$. For detailed discussions of the BLM refer to Ref. 8.

Introducing the heat content density $h(s,t)$ as a dynamical variable

$$h(s,t)=wl=w^2/v_n \ , \tag{2.2}$$

where $w \equiv u_s/\Delta$, we can write down its evolution equation as

$$\left.\frac{\partial h(s,t)}{\partial t}\right|_n = v_n(1-\Delta w)-v_n hk+\frac{1}{\Delta^2}\frac{\partial}{\partial s}\frac{h}{w}\frac{\partial w}{\partial s} \ . \tag{2.3}$$

The modified Gibbs-Thomson boundary condition Eq. (1.1c) now reads

$$w=1-\Delta^2\alpha(\theta)k-\beta(\theta)v_n \ , \tag{2.4}$$

where $\alpha(\theta)$ and $\beta(\theta)$ incorporate the crystalline anisotropy into the surface-tension and kinetic-growth term, respectively.

We assume the fourfold symmetry of the growth and write

$$\alpha(\theta)=1-\epsilon_s \cos 4\theta \tag{2.5a}$$

and

$$\beta(\theta)=\epsilon_k \Delta^4(1-\cos 4\theta) \ . \tag{2.5b}$$

Our numerical work is done in two cases separately: anisotropy in the kinetic-growth term with $\epsilon_k \neq 0$, $\epsilon_s = 0$ and anisotropy in the surface-tension term with $\epsilon_s \neq 0$, $\epsilon_k = 0$.

Equations (2.1)–(2.5) completely determine the interface motion in BLM. All the quantities are written in dimensionless form, and are related to the physical quantities, denoted by capital letters, through the scaling $k=d_0K/\Delta^3$, $h=\Delta^3 H/d_0$, $s=\Delta^3 S/d_0$, $t=\Delta^8 DT/d_0^2$, and $v=d_0V/(D\Delta^5)$.

We now write the equations in s coordinate and θ coordinate using the relation

$$\left.\frac{\partial}{\partial t}\right|_s = \left.\frac{\partial}{\partial t}\right|_n - \int_0^s k v_n ds' \frac{\partial}{\partial s} \tag{2.6}$$

and

$$\left.\frac{\partial}{\partial t}\right|_\theta = \left.\frac{\partial}{\partial t}\right|_n + k\frac{\partial v_n}{\partial \theta}\frac{\partial}{\partial \theta} \ . \tag{2.7}$$

Equations (2.1a) and (2.3) become

$$\left.\frac{\partial h}{\partial t}\right|_s = v_n(1-\Delta w)-kw^2+\frac{1}{\Delta^2}\frac{\partial}{\partial s}\frac{h}{w}\frac{\partial w}{\partial s} - \frac{\partial h}{\partial s}\int_0^s k v_n ds' \ , \tag{2.8a}$$

$$\left.\frac{\partial k}{\partial t}\right|_s = -\left[k^2+\frac{\partial^2}{\partial s^2}\right]v_n - \frac{\partial k}{\partial s}\int_0^s k v_n ds' \tag{2.8b}$$

in the s representation and

$$\left.\frac{\partial h}{\partial t}\right|_\theta = v_n(1-\Delta w) - kw^2 + \frac{k}{\Delta^2}\frac{\partial}{\partial\theta}\left[\frac{hk}{w}\frac{\partial w}{\partial\theta}\right] + k\frac{\partial v_n}{\partial\theta}\frac{\partial h}{\partial\theta}\ , \tag{2.9a}$$

$$\left.\frac{\partial k}{\partial t}\right|_\theta = -k^2\left[1+\frac{\partial^2}{\partial\theta^2}\right]v_n \tag{2.9b}$$

in the θ representation.

As it turns out, working in the θ coordinate is much more convenient than the s coordinate due to the absence of integrals in Eq. (2.8). The two coordinates are connected by the transformation $k=\partial\theta/\partial s$. When k is larger than zero, the correspondence between s and θ is single valued. This is indeed true for an infinitesimal perturbation around a needle crystal. The physical results are independent of the specific choice. What is important is that in both cases we are doing the linear-stability analysis in the moving frame of the needle crystal and not in the laboratory frame.

The needle-crystal steady-state solution $h^*(\theta), k^*(\theta), \ldots$ obtained by setting in Eq. (2.9)

$$\left.\frac{\partial h^*}{\partial t}\right|_\theta = 0, \quad \left.\frac{\partial k^*}{\partial t}\right|_\theta = 0 \tag{2.10}$$

is known, in general, only numerically. Now we consider small time-dependent perturbations to the steady-state solution. We perform the expansion

$$h(\theta,t) = h^*(\theta) + \tilde{h}(\theta,t)\delta + O(\delta^2)\ , \tag{2.11a}$$

$$k(\theta,t) = k^*(\theta) + \tilde{k}(\theta,t)\delta + O(\delta^2)\ , \tag{2.11b}$$

where δ is a small quantity, introduced here for bookkeeping purposes only. Plugging Eq. (2.11) into Eq. (2.9), and keeping only terms linear in δ, we obtain the linear-stability equation

$$\left.\frac{\partial\tilde{k}}{\partial t}\right|_\theta = -k^2\left[1+\frac{\partial^2}{\partial\theta^2}\right]\tilde{v}_n\ , \tag{2.12a}$$

and

$$\begin{aligned}\left.\frac{\partial\tilde{h}}{\partial t}\right|_\theta =& (1-\Delta w)\tilde{v}_n - (\Delta v_n + 2wk)\tilde{w} - w^2\tilde{k} + \frac{\partial v_n}{\partial\theta}\frac{\partial h}{\partial\theta}\tilde{k} \\ &+ k\frac{\partial h}{\partial\theta}\frac{\partial\tilde{v}_n}{\partial\theta} + k\frac{\partial v_n}{\partial\theta}\frac{\partial\tilde{h}}{\partial\theta} + \frac{1}{\Delta^2}\frac{\partial}{\partial\theta}\left[\frac{hk}{w}\frac{\partial w}{\partial\theta}\right]\tilde{k} \\ &+ \frac{k}{\Delta^2}\frac{\partial}{\partial\theta}\left[\frac{hk}{w}\frac{\partial\tilde{w}}{\partial\theta}\right] + \frac{k}{\Delta^2}\frac{\partial}{\partial\theta}\left[\frac{k\tilde{h}}{w}\frac{\partial w}{\partial\theta}\right] \\ &+ \frac{k}{\Delta^2}\frac{\partial}{\partial\theta}\left[\frac{h\tilde{k}}{w}\frac{\partial w}{\partial\theta}\right] - \frac{k}{\Delta^2}\frac{\partial}{\partial\theta}\left[\frac{hk\tilde{w}}{w^2}\frac{\partial w}{\partial\theta}\right]\ .\end{aligned} \tag{2.12b}$$

We have omitted the superscript $*$ in the steady-state solutions. The tilded quantities are first-order perturbations to the steady-state quantities. Equation (2.12) describes the time evolution of small perturbations as seen in the frame moving with the needle crystal.

For simplicity, instead of using $\tilde{h}$ and $\tilde{k}$, we use $\tilde{k}$ and $\tilde{\phi}$ as our independent field variables, where

$$x = \tan\theta\ , \tag{2.13}$$

$$\tilde{\phi}(x,t) = \frac{\tilde{v}_n(\theta,t)}{\cos\theta}\ . \tag{2.14}$$

After some lengthy algebra, Eq (2.12) can now be written as

$$\frac{\partial\tilde{k}(x,t)}{\partial t} = -k^2(1+x^2)^{3/2}\frac{\partial^2\tilde{\phi}}{\partial x^2}\ , \tag{2.15a}$$

$$\begin{aligned}\frac{\partial\tilde{\phi}(x,t)}{\partial t} =& C_1(x)\frac{\partial^2\tilde{\phi}}{\partial x^2} + C_2(x)\frac{\partial\tilde{\phi}}{\partial x} + C_3(x)\tilde{\phi} \\ &+ C_4(x)\frac{\partial^2\tilde{k}}{\partial x^2} + C_5(x)\frac{\partial\tilde{k}}{\partial x} + C_6(x)\tilde{k}\ .\end{aligned} \tag{2.15b}$$

Here $C_i(x)$ are functions of the steady-state solution $h(x), k(x), \ldots$ and their first- and second-order derivatives, which can be calculated numerically.

We seek solutions to the linearized equations of the form

$$\begin{bmatrix}\tilde{k}(x,t)\\ \tilde{\phi}(x,t)\end{bmatrix} \sim \exp(\lambda t)\begin{bmatrix}\tilde{k}(x)\\ \tilde{\phi}(x)\end{bmatrix}\ . \tag{2.16}$$

The eigenvalue spectrum $\{\lambda\}$ solved under appropriate boundary conditions determines the linear stability of the steady-state needle crystal under consideration.

The needle crystal is said to be linearly stable only when all the eigenvalues in $\{\lambda\}$ satisfy $\mathrm{Re}(\lambda)<0$, which means that perturbations will decrease with time. On the other hand, if there is certain eigenvalue λ which has $\mathrm{Re}(\lambda)>0$, then the small perturbations will grow with time so as to make the needle crystal linearly unstable.

III. LINEAR STABILITY FOR THE IVANTSOV SOLUTION

Before we present the stability analysis for nonzero surface tension and anisotropy we first discuss the special case of the Ivantsov solution and its linear-stability spectrum. This calculation can be done analytically and was first performed by Goldenfeld and Langer.[19]

In the absence of surface tension and crystalline anisotropy, $\alpha(\theta)=\beta(\theta)=0$ in Eq. (2.4), the BLM recovers the continuum of the Ivantsov solution. In this case $w=1$, $h=1/v_n$, and Eq. (2.9) takes the form

$$\left.\frac{\partial h}{\partial t}\right|_\theta = (1-\Delta)v_n - k + k\frac{\partial v_n}{\partial\theta}\frac{\partial h}{\partial\theta}\ . \tag{3.1}$$

Using Eq. (2.10), which implies $v_n = v_0\cos\theta$, we find the steady-state solution

$$k^*(\theta) = v_0(1-\Delta)\cos^3\theta\ , \tag{3.2}$$

where v_0 can take an arbitrary value from zero to infinity. These solutions form the Ivantsov continuum, representing parabolic fronts translating uniformly with velocity v_0.

To study the linear stability of the Ivantsov solution we proceed in a similar way to that sketched in Sec. II to find the linear-stability equation. The coefficients C_i in Eq. (2.15) now have simple analytic forms. Equation (2.15) becomes

$$\frac{\partial\tilde{k}(x,t)}{\partial t}=-v_0^2(1-\Delta)^2(1+x^2)^{-3/2}\frac{\partial^2\tilde{\phi}(x,t)}{\partial x^2}\ , \tag{3.3a}$$

$$\frac{\partial\tilde{\phi}(x,t)}{\partial t}=\frac{v_0^2(1-\Delta)}{(1+x^2)}\left[\frac{(1+x^2)^{3/2}}{(1-\Delta)}\tilde{k}(x,t)-2x\frac{\partial\tilde{\phi}(x,t)}{\partial x}-\tilde{\phi}(x,t)\right]\ . \tag{3.3b}$$

Inserting Eq. (3.3b) into Eq. (3.3a) with the use of Eq. (2.16), we get

$$\frac{d^2\tilde{\phi}(x)}{dx^2}+2\lambda x\frac{d\tilde{\phi}(x)}{dx}+[\lambda+\lambda^2(1+x^2)]\tilde{\phi}(x)=0\ , \tag{3.4}$$

where the eigenvalue λ has been rescaled in units of $v_0^2(1-\Delta)$, the inverse of the characteristic time for the needle crystal to travel a distance of one tip radius.

Letting $\tilde{\phi}(x)=\exp(-\lambda x^2/2)f(x)$, Eq. (3.4) reduces to

$$\frac{d^2f(x)}{dx^2}+\lambda^2 f(x)=0\ . \tag{3.5}$$

We recognize this to be the equation of motion for a harmonic oscillator. Thus the eigenvalue spectrum is simply a continuum $\{\lambda\}=(-\infty,+\infty)$. The corresponding eigenfunction can be written

$$\tilde{\phi}(x)=[A\sin(\lambda x)+B\cos(\lambda x)]\exp(-\lambda x^2/2) \tag{3.6}$$

for $\lambda\in(-\infty,+\infty)$, where A and B are constants.

We see that the Ivantsov family is totally unstable with a continuum of unstable modes, and the corresponding eigenfunctions are spatially localized.

IV. MATRIX-DIAGONALIZATION METHOD

The most straightforward way of solving the stability equation (2.15) is to discretize it and solve the eigenproblem for the resulting stability matrix. We refer to this method as the matrix method.

We first solve Eq. (2.9) for the steady-state needle-crystal solution, following the method discussed by Ben-Jacob *et al.*[8] The idea is to integrate a set of first-order ordinary differential equations (ODE's) from a fixed point of the system (corresponding to the tail of the needle crystal) until the tip $\theta=0$. Then the condition of reflection symmetry at the tip is imposed, which requires the vanishing of a mismatch function, taken to be $\Gamma(\Delta,\epsilon,v)\equiv(dw/ds)\,|_{s=0}$.

The result is the selection of a discrete set of needle-crystal steady states with their velocities v_i ($i=0,1,2,\ldots$) decreasing with increasing index number i, where v_i is a function of the undercooling Δ and the anisotropy ϵ_s or ϵ_k. This procedure can be performed with an accuracy corresponding to a value of the mismatch function of about 10^{-16}.[18]

Next, we discretize Eq. (2.15) along the needle crystal. The discretization is performed with a uniform spacing in x with N points on half of the needle crystal ranging from the tip ($x=0$) to far into the tail ($x=L$, a cutoff). For most of the runs, we choose $L\sim 5$ corresponding to an arclength of about ten tip radius, which is checked to be long enough for convergence. By this we mean that the continuum modes have converged to being stable and that the discrete modes are insensitive to varying L. This is discussed further below.

The derivatives are discretized using the standard three-point formulas which are accurate to $O(1/N^2)$. Finally, we obtain a $2N\times 2N$ stability matrix M which can be written schematically as

$$\lambda\begin{bmatrix}\tilde{k}(i)\\ \tilde{\phi}(i)\end{bmatrix}_{2N}=\begin{bmatrix}M^{11}_{N\times N} & M^{12}_{N\times N}\\ M^{21}_{N\times N} & M^{22}_{N\times N}\end{bmatrix}_{2N\times 2N}\begin{bmatrix}\tilde{k}(i)\\ \tilde{\phi}(i)\end{bmatrix}_{2N}\ . \tag{4.1}$$

The matrix $M^{11},M^{12},M^{21},M^{22}$ and thus M are calculated numerically from the steady-state solution with appropriate boundary conditions imposed at the tip and tail, namely,

$$\frac{d\tilde{k}(0)}{dx}=\frac{d\tilde{\phi}(0)}{dx}=0,\quad \tilde{k}(L)=\tilde{\phi}(L)=0 \tag{4.2a}$$

for symmetric modes and

$$\tilde{k}(0)=\tilde{\phi}(0)=0,\quad \tilde{k}(L)=\tilde{\phi}(L)=0 \tag{4.2b}$$

for antisymmetric modes.

Truncation of the matrix M can be made in order to minimize the possible boundary effects. We will only report results on the symmetric modes for simplicity; similar results were also obtained for antisymmetric modes with no qualitative physical difference.

Since the matrix M is not symmetric in nature, its eigenvalues are complex-conjugate pairs in general. We used IMSL EIGRF subroutine on the VAX computer and EISPACK RG subroutine on the CRAY computer to perform the matrix diagonalization; both subroutines gave the same results.

Figures 1(a)–1(c) are typical eigenvalue spectra. The eigenvalues are scaled in units of v_0/ρ_0 as in the Ivantsov case. The spectra are totally different from that of the Ivantsov solution because of the nonperturbative nature of the selection mechanism. The spectrum generally consists of three parts.

One is an approximate zero mode in the spectrum whose appearance is due to the translation invariance in the comoving frame of the needle crystal. It is approximate because of both the linearization approximation of our stability operator and the finite numerical accuracy. Its existence has been discussed by Kessler and Levine in the cases of geometrical model[20] (GM) and the Saffman-Taylor problem.[21] This zero mode can serve as a check of the numerical procedure we employed. We have observed zero modes in all our well-converged spectra, the zero mode being more than three orders of magnitude smaller than a typical eigenvalue. For example, in Fig.

1(a), $\lambda_0 = 4.5 \times 10^{-14}$, which is virtually zero.

Another part of the spectrum is the complex continuum which extends to large negative Re(λ) and Im(λ). Eigenvalues are grouped in complex-conjugate pairs. The eigenfunctions of these eigenvalues are extended, with amplitude oscillating and diverging to infinity at the tail of the needle crystal.

This complex continuum is associated with the convective instability as it describes the disturbance advected away from the tip along the needle crystal as seen from the comoving frame. The extended nature of the eigenfunction determines that the spectrum is sensitive to the cutoff length L, as indeed observed in the numerics. As we change L, slight changes in the continuum are observed.

Using the matrix method we have studied the eigenvalue spectrum for $\Delta = 0.75$, $\epsilon_k \geq 0.03$, and $\epsilon_s \geq 0.04$. No continuum instabilities are observed, i.e., all Re(λ) < 0.

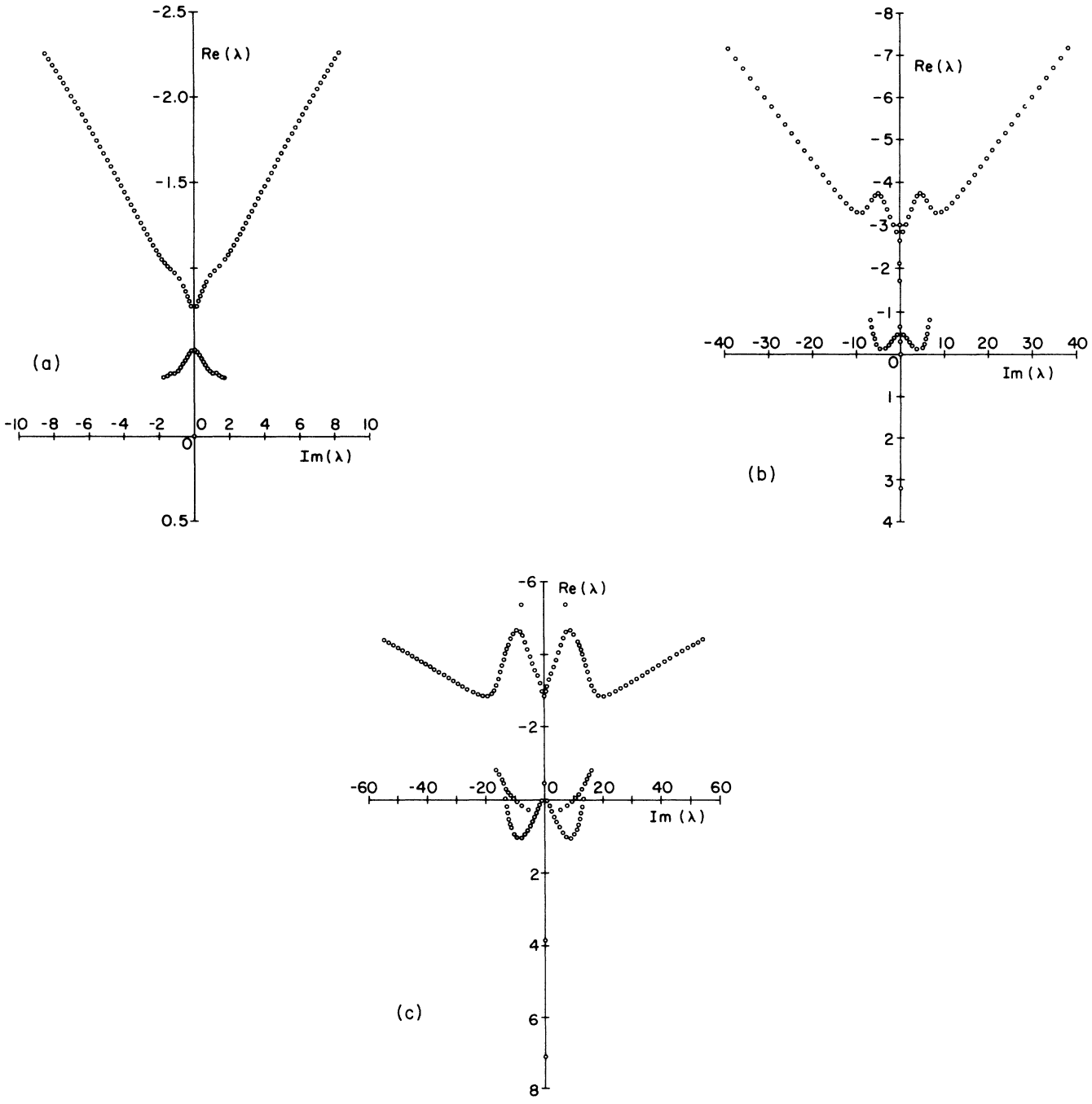

FIG. 1. Eigenvalue spectra for the needle-crystal solutions with velocity v_i ($i = 0, 1, 2, 3, \ldots$) at $\Delta = 0.75$, $\epsilon_k = 0.3$, $\epsilon_s = 0$. (a) is the spectrum for the fastest-moving needle crystal $i = 0$, with no unstable mode; (b) is the spectrum for slower needle crystal $i = 1$, with one unstable discrete mode at 3.21; (c) is the spectrum for needle crystal $i = 2$, with two unstable modes at 7.13 and 3.86.

For smaller ϵ_k or ϵ_s, the convergence of the continuum part becomes poorer. The computation is extremely hard to implement because of the rising CPU time needed to keep reasonable numerical accuracy. There are two main reasons for this difficulty.

Firstly, in order to get the physical spectrum, the discretization length ds must be smaller than the characteristic stability length $l_s=2\pi(d_0 l)^{1/2}$, or $ds<l_s$. We know that l_s scales with v_0 as

$$l_s \sim \frac{1}{v_0^{1/2}} .$$

On the other hand, the tip radius scales with v_0 roughly as

$$\rho_0=\frac{1}{k_0}\sim\frac{1}{v_0} .$$

So after all, the number of necessary discretization points scales as

$$N\sim\frac{\rho_0}{ds}>\frac{\rho_0}{l_s}\sim v_0^{-1/2} ,$$

which diverges for vanishingly small anisotropy when $v_0\to 0$.

The second reason is the possible noise amplification due to the nonlinear effect. It is possible that the fastest needle crystal is linearly stable but may have a nonlinear instability with exponentially vanishing threshold amplitude. This scenerio was suggested by Bensimon[22] in the context of Saffman-Taylor fingers. Assuming this nonlinear instability, very small numerical noise or inaccuracy may get amplified so as to make the continuum unstable.

The third part of the eigenspectrum, which is the most interesting one, consists of discrete eigenvalues. They are always real and may lie both on the positive and negative real axes. The positive real eigenvalues correspond to the absolute instability of the interface; i.e., such modes cannot be made to appear stable by transforming to some different reference frame. Their eigenfunctions are localized around the needle-crystal tip, so the existence of such positive real eigenvalues implies the tip-splitting instability of the interface.

We list the velocities, tip curvatures, and the discrete unstable eigenvalues for different members of the needle crystal family $\{v_i\}$ at $\Delta=0.75$, $\epsilon_k=0.3$, $\epsilon_s=0$:

$$v_0=4.40\times10^{-1},\quad k_0(0)=2.53\times10^{-1},\quad \lambda=\{\text{none}\} ,$$
$$v_1=9.80\times10^{-2},\quad k_1(0)=2.37\times10^{-2},\quad \lambda=\{3.21\} ,$$
$$v_2=2.35\times10^{-2},\quad k_2(0)=5.89\times10^{-3},\quad \lambda=\{3.86,7.13\} ,$$
$$v_3=7.40\times10^{-3},\quad k_3(0)=1.85\times10^{-3},\quad \lambda=\{4.58,8.54,12.0\} .$$

The corresponding spectra are shown in Fig. 1. We should note that in Fig. 1(c) there is a continuum part lying in the right half of the complex plane. This is due to the numerical difficulty as we discussed previously. The continuum should converge completely to the stable region if we compute more accurately using larger matrices. For this same reason, the eigenvalue 4.58 for v_3 is not well converged and should be smaller. The eigenfunctions of some of these unstable modes are plotted in Fig. 2. As can be seen, they are truly localized and represent the tip-splitting instability of the interface. Calculations were also done for $0.90>\Delta>0.65$ and $\epsilon_k>0.1$ with qualitatively the same result.

Results for anisotropy in the surface-tension term at $\Delta=0.75$, $\epsilon_s=0.40$ are also given below, which are similar to those for kinetic-term anisotropy:

$$v_0=0.580,\quad k_0(0)=0.341,\quad \lambda=\{\text{none}\} ,$$
$$v_1=1.43\times10^{-1},\quad k_1(0)=3.18\times10^{-2},\quad \lambda=\{3.72\} ,$$
$$v_2=5.35\times10^{-2},\quad k_2(0)=1.35\times10^{-2},\quad \lambda=\{3.53,7.05\} .$$

From these results, we find that the ith needle crystal is unstable with i unstable discrete eigenmodes. The fastest-moving needle crystal (or the zeroth) is linearly stable. This result agrees with those of Kessler and Levine[15] and Bensimon *et al.*[13]

We cannot exclude the possibility that the fastest-moving needle crystal v_0 has a discrete mode instability for smaller anisotropies than those used above. At the smallest anisotropies used above, the wavelength of the most unstable mode of a planar interface moving along its normal at the speed v_0 is about four times smaller than the tip radius. To push the calculation to anisotropies smaller than $\epsilon_k=0.03$ and $\epsilon_s=0.04$ we have used the shooting method, discussed in Sec. V.

V. DIFFERENTIAL-EQUATION INTEGRATION METHOD

In this section we study the discrete mode instability using the differential-equation integration (shooting) method first used by Mack[16] to study the Orr-Sommerfeld equation. The method was later used by Kessler, Koplik, and Levine[6] in studying the GM of solidification. The method involves the separation of the original stability equation (2.15) into a set of first-order ordinary differential equations on which the numerical integration can be performed. The eigenvalues are selected in order to satisfy certain boundary conditions. For a detailed discussion the reader is referred to Ref. 16.

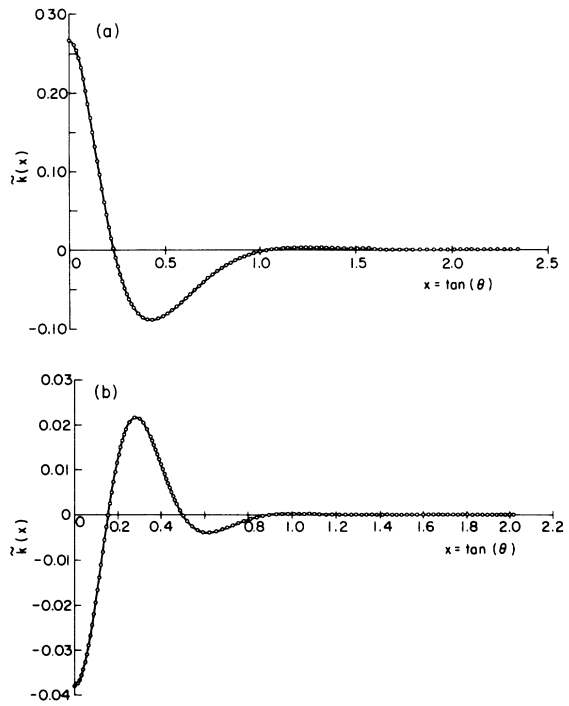

FIG. 2. Eigenfunctions of the unstable modes in Fig. 1. (a) Eigenfunction $\tilde{k}(x)$ for mode 3.21 in Fig. 1(b); (b) eigenfunction $\tilde{k}(x)$ for mode 7.13 in Fig. 1(c).

The advantage of this shooting method is in that it gets rid of the heavy algebratic matrix operations encountered in the matrix method and thus saves a lot of computing time. It is more than one order of magnitude faster than the matrix method and can be made very accurate. The only sacrifice is the complication of formulating the problem.

Introducing $\tilde{e}(x)=d\tilde{k}(x)/dx$ and $\tilde{g}(x)=d\tilde{\phi}(x)/dx$, the linear-stability equation (2.15) along with Eq. (2.16) reduces to the four first-order differential equations:

$$\frac{d\tilde{k}(x)}{dx}=\tilde{e}(x)\ , \tag{5.1a}$$

$$\frac{d\tilde{\phi}(x)}{dx}=\tilde{g}(x)\ , \tag{5.1b}$$

$$\frac{d\tilde{g}(x)}{dx}=-\frac{\lambda}{k^2(1+x^2)^{3/2}}\tilde{k}(x)\ , \tag{5.1c}$$

$$\frac{d\tilde{e}(x)}{dx}=\frac{\lambda k^{-2}(1+x^2)^{-3/2}C_1-C_6}{C_4}\tilde{k}(x) + \frac{\lambda-C_3}{C_4}\tilde{\phi}(x)-\frac{C_2}{C_4}\tilde{g}(x)-\frac{C_5}{C_4}\tilde{e}(x)\ . \tag{5.1d}$$

These four equations are an alternative way of writing the two second-order stability equations. Notice that λ is a complex number in general, hence, $\tilde{k},\tilde{\phi},\tilde{g},\tilde{e}$ are all complex functions.

The boundary conditions are now

$$\tilde{k}(x),\tilde{\phi}(x),\tilde{g}(x),\tilde{e}(x)\to 0 \quad \text{as } x\to\infty\ , \tag{5.2a}$$

along with

$$\tilde{k}(0)=0,\quad \tilde{\phi}(0)=0$$

for antisymmetric modes and

$$\tilde{g}(0)=0,\quad \tilde{e}(0)=0 \tag{5.2b}$$

for symmetric modes. We can find the asymptotic solution of Eq. (5.1) at large $x\to\infty$ using the WKB method. There are four linearly independent sets of solutions:

$$\tilde{\phi}(x)_{1,2}\sim\exp[-\tfrac{1}{2}\lambda x^2\pm i\lambda x+O(\sqrt{v_0})] \tag{5.3a}$$

and

$$\tilde{\phi}(x)_{3,4}\sim\exp\left[\frac{1}{2}\lambda x^2+\frac{\Delta^2}{2(1-\Delta)}x^2\pm\frac{2i\sqrt{v_0}}{5(1-\Delta)}x^{5/2} +O(\sqrt{v_0})\right]\ . \tag{5.3b}$$

Expressions for $\tilde{k},\tilde{g},\ldots$ are not listed since they have the same large x exponential behavior. Since we are only interested in the *unstable* discrete modes with $\mathrm{Re}(\lambda)>0$, we find that only solutions Eq. (5.3a) satisfy the boundary condition equation (5.2a) while solutions Eq. (5.3b) diverge at large x and fail to satisfy boundary condition equation (5.2a).

Solutions Eq. (5.3a) provide the initial conditions for our numerical integration of Eq. (5.1), which proceed from a large finite value of $x=L$ to the tip at $x=0$, with a step length dx. Coefficients in Eq. (5.1) are calculated numerically from the needle-crystal solution at every integration step.

We use the notation that $S_1=(\tilde{k}_1,\tilde{\phi}_1,\tilde{g}_1,\tilde{e}_1)$ and $S_2=(\tilde{k}_2,\tilde{\phi}_2,\tilde{g}_2,\tilde{e}_2)$ for the two sets of linear independent solutions in Eq. (5.3a). Both S_1 and S_2 are integrated simultaneously, which makes a total of eight complex or 16 real first-order ODE's. We use the double precision differential-equation solver DGEAR in the IMSL software package on the VAX. Both the implicit Adams method and Gear's stiff method are used with choices of different iteration methods. We compare results from different methods to check the correctness of our computer codes and check if our problem is stiff, as it should not be. For most of the work, the Adams method is used.

The admixture of solution S_1 with S_2 and with those in Eq. (5.3b) due to the computational roundoff errors tends to destroy the linear independence of the S_1 and S_2 solutions. Thus the Gram-Schmidt orthonormalization procedure is employed after each integration step to keep this independence. To save computer time, orthonormalization can be done every several steps instead of one.

The solution vectors after orthonormalization are denoted by S_1^{new} and S_2^{new}, where

$$S_1^{\text{new}}=S_1/(S_1^*\cdot S_1)^{1/2}\ , \tag{5.4a}$$

$$S_2^{\text{new}}=\frac{[S_2-(S_1^{\text{new}*}\cdot S_2)S_1^{\text{new}}]}{|S_2-(S_1^{\text{new}*}\cdot S_2)S_1^{\text{new}}|}\ . \tag{5.4b}$$

At the tip of the needle crystal, $x=0$, the solution $(\tilde{k}(0),\tilde{\phi}(0),\tilde{g}(0),\tilde{e}(0))$ is the linear combination of the two independent solutions S_1 and S_2 at $x=0$.

The enforcement of the boundary condition equation

(5.2) leads to two complex secular determinant equations:

$$\mathcal{D}(\lambda)=\begin{vmatrix}\tilde{g}_1(0) & \tilde{g}_2(0)\\ \tilde{e}_1(0) & \tilde{e}_2(0)\end{vmatrix}=0 \tag{5.5a}$$

for symmetric modes and

$$\mathcal{D}(\lambda)=\begin{vmatrix}\tilde{k}_1(0) & \tilde{k}_2(0)\\ \tilde{\phi}_1(0) & \tilde{\phi}_2(0)\end{vmatrix}=0 \tag{5.5b}$$

for antisymmetric modes.

Integrations are performed for different λ values in the complex plane to search for those which satisfy Eq. (5.5). Again, we report results on symmetric modes only for simplicity. In actually carrying out the searching, we choose different λ values, integrate Eq. (5.1), and thence obtain the value $\mathcal{D}(\lambda)$. Then we plot contours of $\mathrm{Re}\mathcal{D}(\lambda)=0$ and $\mathrm{Im}\mathcal{D}(\lambda)=0$ on the complex λ plane, where $\mathrm{Re}\mathcal{D}$ and $\mathrm{Im}\mathcal{D}$ are real and imaginary parts of $\mathcal{D}(\lambda)$, respectively. The eigenvalues are the intersection points of the real contours and the imaginary contours. Equation (5.1) is solved only on the right half of the complex λ plane because that is where the unstable modes may be.

Figure 3 shows the contour diagrams of the fastest-moving needle crystal with index $i=0$ at $\epsilon_k=0.20$ [Fig. 3(a)] and the next fastest needle with index $i=1$ at $\epsilon_k=0.30$ [Fig. 3(b)]. We see from Fig. 3 that there are *no* intersection points *outside* the real axis [where $\mathrm{Im}(\lambda)\neq 0$]. In other words, all the unstable modes must be purely real. We have checked this for different Δ and $\epsilon_{s,k}$. This can also be seen from the spectra obtained using the matrix method.

With this result, we can simply assume λ to be real and do the shooting for λ on the positive real axis only, which simplifies our numerical procedure substantially. When λ is taken real, $\mathrm{Im}\mathcal{D}(\lambda)\equiv 0$, the eigenvalues are simply zeros of the real equation

$$\mathrm{Re}\mathcal{D}(\lambda)=0\ . \tag{5.6}$$

In Fig. 4 we plot the $\mathcal{D}(\lambda)$ as a function of λ for the needle-crystal family $\{v_i\}$ with $i=0,1,2,3$ at $\Delta=0.75$, $\epsilon_k=0.30$, $\epsilon_s=0$. Discrete unstable eigenmodes are given below:

$$v_0=4.40\times 10^{-1},\quad \lambda=\{\text{none}\}\ ,$$
$$v_1=9.80\times 10^{-2},\quad \lambda=\{3.21\}\ ,$$
$$v_2=2.35\times 10^{-2},\quad \lambda=\{3.82,7.08\}\ ,$$
$$v_3=7.40\times 10^{-3},\quad \lambda=\{4.25,8.35,11.9\}\ .$$

Eigenvalues for anisotropy in surface-tension term at $\Delta=0.75$, $\epsilon_s=0.40$ are

$$v_0=0.580,\quad \lambda=\{\text{none}\}\ ,$$
$$v_1=1.43\times 10^{-1},\quad \lambda=\{3.71\}\ ,$$
$$v_2=5.35\times 10^{-2},\quad \lambda=\{3.51,7.04\}\ .$$

Again, as in the matrix method, we find that there are i zeros of $\mathcal{D}(\lambda)$ on the positive real axis and thus there are i unstable modes for the needle crystal with index i.

We can compare these eigenvalues with those obtained using the matrix method in Sec. IV. The agreement is remarkable, better than 3%, except for the smallest eigenvalue in v_3, which is not well converged. This agreement gives us confidence in our numerical procedure and we may safely go to smaller anisotropies for the fastest-moving needle crystal.

Figure 5 plots the $\mathcal{D}(\lambda)$ versus λ curves for different anisotropies $0.35\geq\epsilon_k,\epsilon_s\geq 0.01$ at $\Delta=0.75$. As can be seen, the curves are monotonic in λ, and no zero is found on the positive real axis, which means that the needle crystal is linearly stable for anisotropies as low as 0.01. Smaller anisotropy is unaccessible because the velocity v_0 gets so small (less than 10^{-3}) that it is extremely hard to get the steady-state solution with reasonable accuracy. At the same time, shooting also gets more time consuming. At this value of the anisotropy, the wavelength of the most unstable mode for a planar interface moving

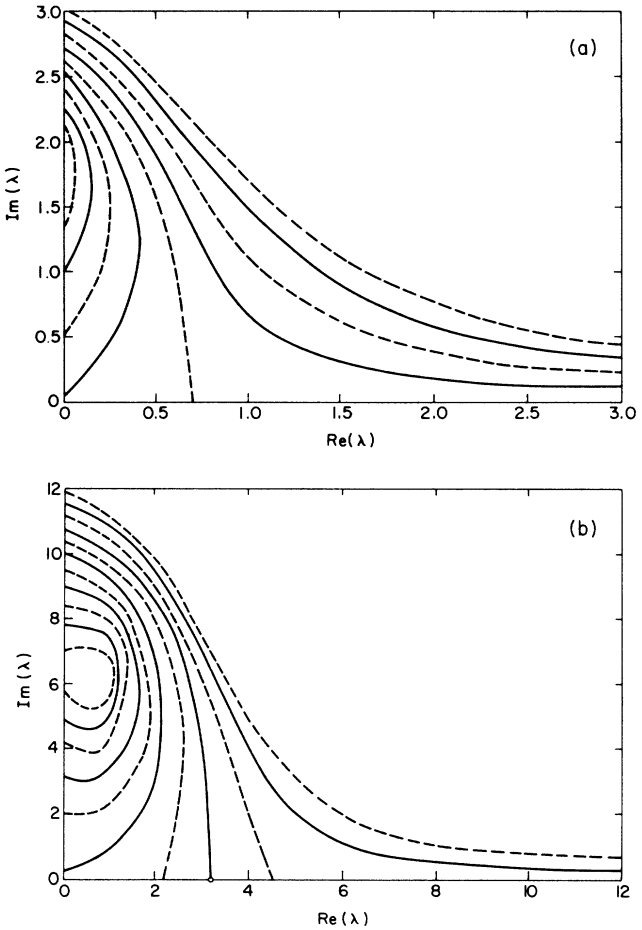

FIG. 3. Contours of $\mathrm{Im}\mathcal{D}(\lambda)=0$ (dashed line) and $\mathrm{Re}\mathcal{D}(\lambda)=0$ (solid line). Only the upper half plane is plotted due to the invariance of $\mathcal{D}(\lambda)$ under the reflection $\lambda\rightarrow\lambda^*$. Note also that on the real axis, $\mathrm{Im}\mathcal{D}(\lambda)\equiv 0$. There is (a) for the fastest-moving needle crystal at $\Delta=0.75$, $\epsilon_k=0.2$ no intersection point between $\mathrm{Im}\mathcal{D}=0$ and $\mathrm{Re}\mathcal{D}=0$; (b) for the needle crystal with index $i=1$ at $\Delta=0.75$, $\epsilon_k=0.3$ one intersection point on the positive real axis at 3.21.

along its normal with speed v_0 is about one tenth of the tip radius.

However, we can plot the data in another way to do the extrapolation. To do this, we plot the quantity $1/|\ln\mathcal{D}(0)|$ as a function of ϵ_s, ϵ_k, where $\mathcal{D}(0)$ is the intercept $\mathcal{D}(\lambda=0)$. This is shown in Fig. 6, from which we can reasonably conclude that the intercept $\mathcal{D}(0)>0$ for all $\epsilon_{s,k}>0$. In turn, $\mathcal{D}(\lambda)>0$ for all $\lambda>0$; this asserts the absence of discrete mode instability for the needle crystal at all nonzero anisotropies.

VI. DISCUSSION

Let us summarize our main results as follows.

We have shown that the ith selected needle-crystal steady state with velocity v_i ($i=1,2,\ldots$) is unstable into i tip-splitting discrete modes. (Actually there are also i unstable antisymmetric modes, making a total of $2i$ modes.) This picture is consistent with the observation by Bensimon *et al.*[13] in their WKB approach and by Kessler and Levine[15] in their numerical work.

The first needle-crystal solution (or the fastest moving one) is free of any discrete mode instability. This we have shown to be true for $\epsilon_{s,k}\geq 0.01$ and extrapolated to all nonvanishing anisotropies. The absence of continuum (which we presume is a convective instability) is established numerically for $\epsilon_{s,k}\geq 0.03$. It is believed that the continuum does not play an important role regarding the linear stability of the needle crystal. The conclusion is then that the fastest-moving needle crystal is linearly stable for all nonvanishing anisotropy strength.

We should mention that this result is in disagreement with the direct time-dependent numerical simulations of the BLM. In a recent paper by Pieters,[17] time-dependent simulations are performed. The method is to put small perturbations (say, a bump) on the needle-crystal solution at time zero and then let the system evolve in time. The motion of the perturbations is monitored to determine if the needle is stable against the perturbation. Instabilities are observed for anisotropies below a critical value. The same scenario had also been observed by Martin and Goldenfeld.[18]

However, we believe that these observations are the results of the possible nonlinear instability as discussed in

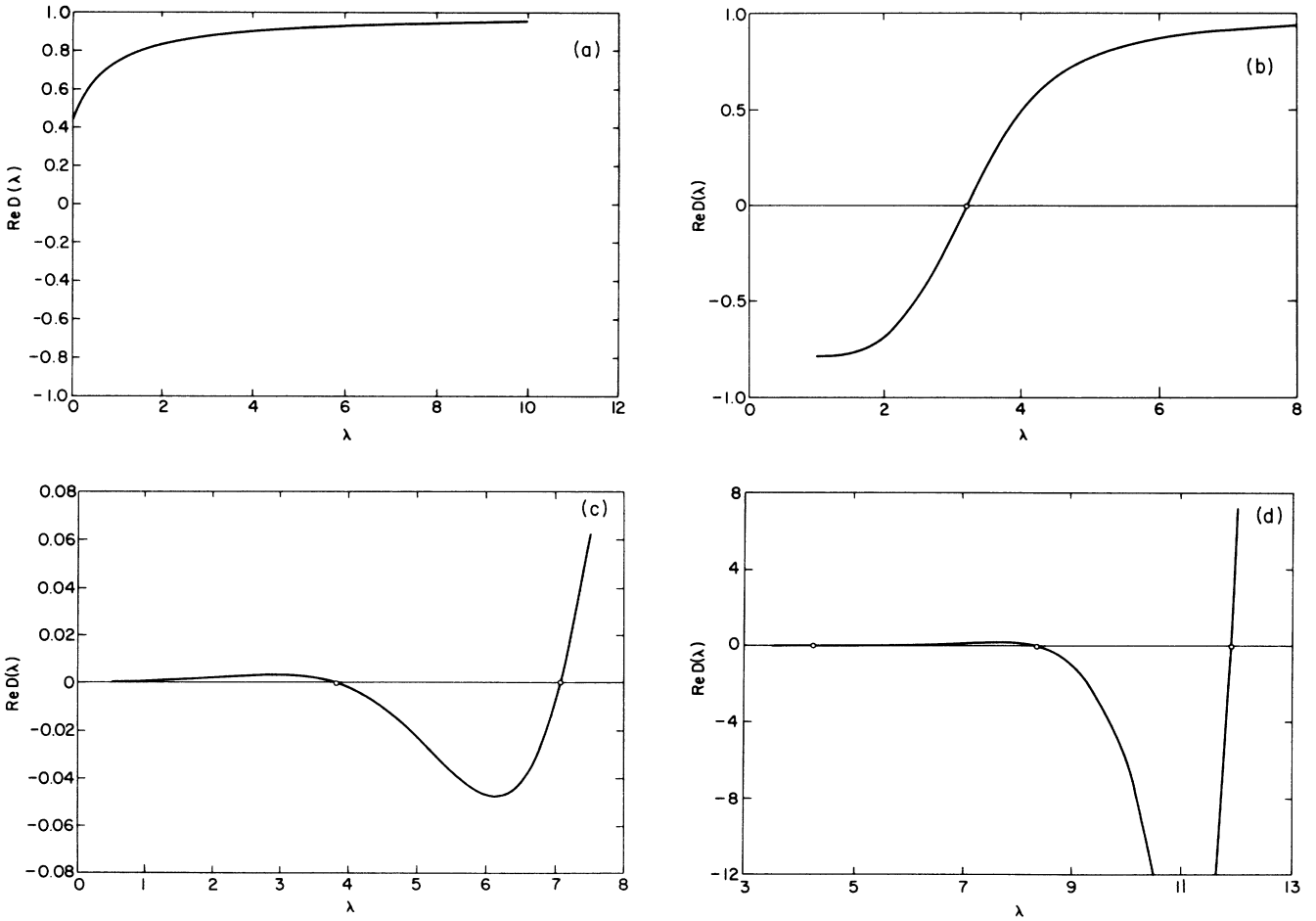

FIG. 4. $\mathrm{Re}\mathcal{D}(\lambda)$ vs λ for the needle-crystal solutions v_i ($i=0,1,2,\ldots$) at $\Delta=0.75$, $\epsilon_k=0.3$, $\epsilon_s=0$. λ is taken real. $\mathrm{Re}\mathcal{D}(\lambda)$ has (a) no zero for the fastest moving needle $i=0$; (b) one zero at 3.21 for the needle crystal with index number $i=1$; (c) two zeros at 7.08 and 3.82 for the needle with index $i=2$; (d) three zeros at 11.89, 8.35, and 4.25 for the needle with index $i=3$. Here the vertical scale is amplified by 10^5.

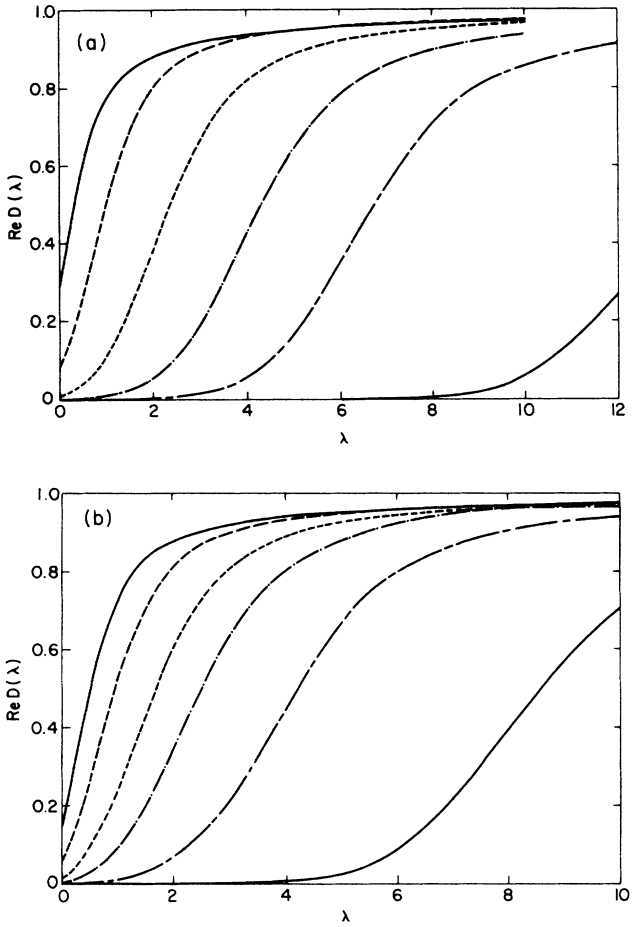

FIG. 5. $\mathcal{D}(\lambda)$ vs ϵ for the fastest needle crystal at different anisotropies, $\Delta=0.75$. (a) Anisotropy in the surface-tension term, curves from left to right are for $\epsilon_s=0.20$, 0.10, 0.05, 0.03, 0.02 and 0.01; (b) anisotropy in the kinetic term, curves from left to right are for $\epsilon_k=0.10$, 0.07, 0.05, 0.04, 0.03, and 0.02.

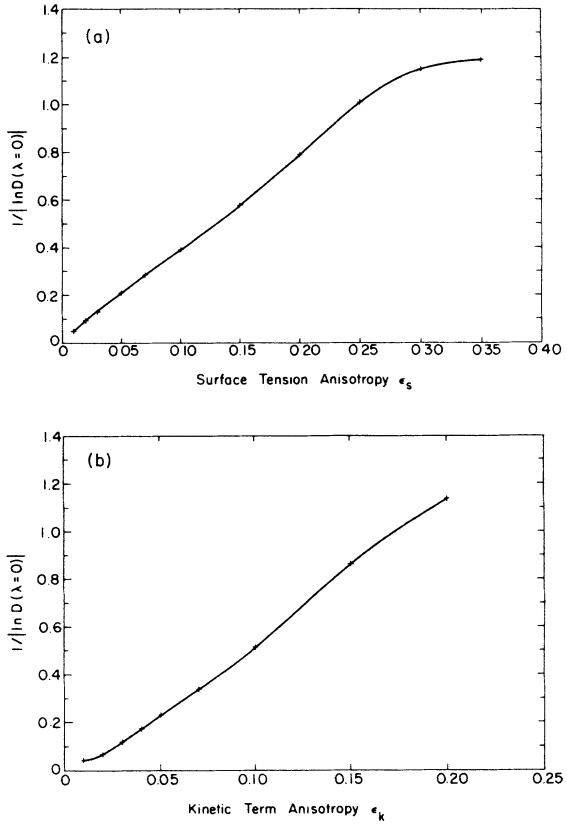

FIG. 6. Figure of $1/|\ln\mathcal{D}(\lambda=0)|$ as a function of anisotropy ϵ. The solid line is the extrapolation. (a) Anisotropy in surface-tension term, $\epsilon_s\neq0$, $\epsilon_k=0$; (b) anisotropy in kinetic term, $\epsilon_k\neq0$, $\epsilon_s=0$.

Sec. IV. At small anisotropy, the threshold amplitude for the onset of nonlinear instability can be exponentially small as suggested by Bensimon for the Saffman-Taylor problem, so a tiny small perturbation may soon ignite the nonlinear instability and drive the system outside the linear regime where our results are meaningful.

As a check, we chose parameter values which are in the region claimed to be unstable by Pieters, for example, $\Delta=0.80$, $\epsilon_s=0.04$, $\epsilon_k=0$. We solved for the spectrum using both the matrix and shooting methods. We found the needle crystal to be linearly stable.

Of course, a detailed study using more accurate time-dependent simulations is needed to confirm the presence of a nonlinear instability.

ACKNOWLEDGMENTS

We thank Olivier Martin for many helpful discussions. We are grateful to J. S. Langer, with whom the work reported in Sec. III was performed; N.D.G. thanks the Institute for Theoretical Physics at Santa Barbara for their hospitality. We thank the Materials Research Laboratory Center of Computation and the National Center for Supercomputing Applications at the University of Illinois for the use of their splendid facilities. This work was supported by National Science Foundation Grant No. DMR-83-16981-23 as part of the Advanced Computation Thrust. N.D.G. gratefully acknowledges support from the Alfred P. Sloan Foundation.

[1]J. S. Langer, Rev. Mod. Phys. **52**, 1 (1980).

[2]P. G. Saffman and G. I. Taylor, Proc. R. Soc. London, Ser. A **245**, 312 (1958).

[3]D. Bensimon, L. P. Kadanoff, S. Liang, B. I. Shraiman, and C. Tang, Rev. Mod. Phys. **58**, 977 (1986).

[4]N. D. Goldenfeld, in *Metastability and Incompletely Posed Problems,* edited by S. Antman, J. L. Ericksen, D. Kinderlehrer, and I. Müller (Springer-Verlag, Berlin, 1987); N. D. Goldenfeld, in *Interfacial Phenomena, NATO Advanced Study Institute, Series B: Physics,* edited by M. G. Velarde (Plenum, New York, in press).

[5]D. A. Kessler, J. Koplik, and H. Levine, Adv. Phys. (to be published).

[6]R. C. Brower, D. A. Kessler, J. Koplik, and H. Levine, Phys.

Rev. Lett. **51**, 1111 (1983); Phys. Rev. A **29**, 1335 (1984); see also D. A. Kessler, J. Koplik, and H. Levine, Phys. Rev. A **30**, 2820 (1984); **30**, 3161 (1984); **31**, 1712 (1985).
[7]D. I. Meiron, Phys. Rev. A **33**, 2704 (1986).
[8]E. Ben-Jacob, N. D. Goldenfeld, J. S. Langer, and G. Schön, Phys. Rev. Lett. **51**, 1930 (1984); Phys. Rev. A **29**, 330 (1984); see also J. S. Langer and D. C. Hong, *ibid.* **34**, 1462 (1986).
[9]E. Ben-Jacob, N. D. Goldenfeld, B. G. Kotliar, and J. S. Langer, Phys. Rev. Lett. **53**, 2110 (1984).
[10]G. P. Ivantsov, Dokl. Akad. Nauk. SSSR **58**, 567 (1947).
[11]S. C. Huang and M. E. Glicksman, Acta Metall. **29**, 707 (1981); **29**, 717 (1981); see also M. E. Glicksman, Mater. Sci. Eng. **65**, 45 (1984).
[12]E. Ben-Jacob, R. Godbey, N. D. Goldenfeld, J. Koplik, H. Levine, T. Mueller, and L. M. Sander, Phys. Rev. Lett. **55**, 1315 (1985).
[13]D. Bensimon, P. Pelcé, and B. I. Shraiman, J. Phys. (Paris) **48**, 2081 (1987).
[14]Ya. B. Zel'dovitch, A. G. Istratov, N. I. Kidin, and V. B. Librovitch, Comb. Sci. Tech. **24**, 1 (1980).
[15]D. A. Kessler and H. Levine, Phys. Rev. Lett. **57**, 3069 (1986).
[16]L. M. Mack, J. Fluid. Mech. **73**, 497 (1976).
[17]R. Pieters, Phys. Rev. A **37**, 3126 (1988); see also R. Pieters and J. S. Langer, Phys. Rev. Lett. **56**, 1948 (1986).
[18]O. Martin and N. D. Goldenfeld, Phys. Rev. A **35**, 1382 (1987).
[19]N. Goldenfeld and J. Langer (unpublished).
[20]D. A. Kessler and H. Levine, Phys. Rev. A **33**, 2634 (1986).
[21]D. A. Kessler and H. Levine, Phys. Rev. A **33**, 2621 (1986).
[22]D. Bensimon, Phys. Rev. A **33**, 1302 (1986).